13. ATTITUDE AND ORBIT CONTROL SYSTEM AND PERFORMANCES

The attitude and orbit control system performed two major tasks. During the spin-stabilised phase, it provided a reference for the control of most of the flight-related functions, such as pointing antennas or solar panels, or orienting the apogee boost motor for orbit manoeuvres. During the three-axis stabilised phase, it coped with the most severe attitude requirements imposed by the payload, the attitude constraints being one of the limiting factors for the experimental accuracy demanded. In the framework of these overall tasks, the attitude and orbit control system carried out a variety of specific functions closely linked to the various operational aspects of the mission.

13.1. Functions of the Attitude and Orbit Control System

Spin-Stabilised Phase

During the spin-stabilised phase at the start of the mission, the attitude and orbit control system was involved in the separation of the satellite from the launch vehicle, the apogee boost motor ignition attempts, the perigee raising manoeuvres and sun acquisition. It was designed to provide:

(i) attitude control by maintaining the nutation angle within acceptable limits for all hydrazine propellant fill ratios and an inertia ratio below 1;

(ii) facilities to control the spin rate, employing 5 N hydrazine thrusters;

(iii) attitude information based on data from an Earth/Sun sensor, to allow the satellite attitude to be determined by the ground;

(iv) facilities to control the satellite spin axis by means of the 5 N thrusters;

(v) means to acquire and maintain the satellite east–west geostationary orbital position by means of 5 N hydrazine thrusters (not used in the revised mission);

(vi) means for a complete evacuation of all residual hydrazine propellant at the end of the spin phase;

(vii) back-up facilities to overcome failures, not handled by the ground station, which would lead to loss of the mission.

Three-Axis Stabilised Phase

During the three-axis stabilised phase, the attitude and orbit control system was involved in sun pointing, sensor calibration, scanning law initialisation, and normal operation. It was designed to:

(i) provide a stable sun pointing, by means of sun acquisition sensor data and 20 mN cold-gas thrusters, to enable gyro calibration and star pattern recognition;

(ii) slew the spacecraft rotation axis from the sun-pointing attitude to its position on the nominal scanning law;

(iii) control the satellite attitude, in order to follow the pre-determined scanning law with a maximum error cone semi-angle of 10 arcmin on the spin axis orientation, and a maximum error angle of 10 arcmin around the spin axis;

(iv) estimate the satellite attitude in real time with an accuracy such that the position of the telescope optical axes could be derived with an accuracy of better than 1 arcsec rms (cone semi-angle).

13.2. Equipment Description

The attitude and orbit control subsystem (Figure 13.1) comprised the control law electronics, the control and actuation electronics, the accelerometer package, the Earth/Sun sensor, the sun acquisition sensor, the attitude anomaly detector, the reaction control assembly and the inertial reference unit (the gyro measurement electronics and the gyro package).

Control Law Electronics

The control law electronics was the core of the subsystem. A microprocessor ran the attitude control software and interfaced with the rest of the spacecraft via the on-board data handling bus. Within the attitude and orbit control system, it interfaced with the control and actuation electronics and the gyro measurement electronics. Its main functions were subsystem telecommand and telemetry management, closed-loop attitude control, open-loop attitude manoeuvres, real-time attitude determination and subsystem configuration, and equipment monitoring.

The control law electronics was based on a TI SBP 9989 I^2L 16-bit microprocessor and a memory bank of 16 k PROM and 4 k RAM, with error detection and correction capability (16 bits of data and 6 bits for Hamming code implementation). The unit was internally fully redundant, and main and redundant functions were properly cross-strapped. The main functional blocks were as follows:

(1) telemetry and telecommand electronics: this module performed the on-board data handling bus interface, the acquisition of analogue data, relay status, and telemetry signals from the attitude and orbit control system, timing extraction from on-board data handling bus and distribution to the subsystem, and telecommand handling and distribution to the attitude and orbit control system users;

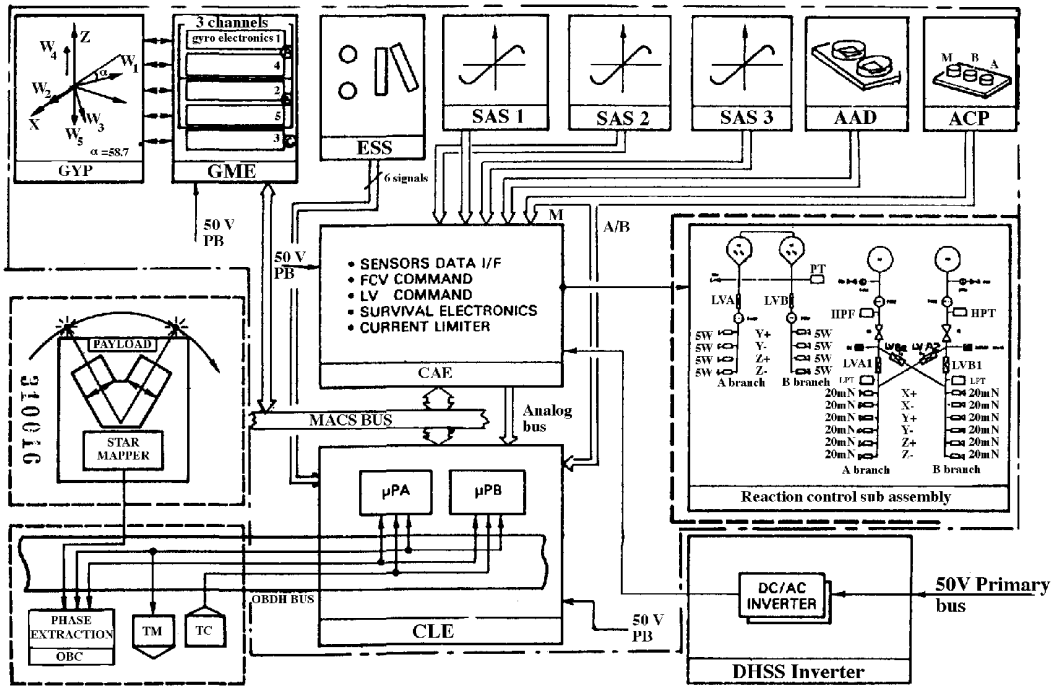

Figure 13.1. *Attitude and orbit control subsystem block diagram, showing the inter-relationship between the various on-board subsystems involved: AAD: attitude anomaly detector; ACP: accelerometer package; CAE: control and actuation electronics; CLE: control law electronics; DHSS: data handling subsytem; ESS: Earth/Sun sensor; GME: gyro mechanism electronics; GYP: gyro package; OBC: on-board computer; SAS: sun acquisition sensor; TM: telemetry; TC: telecommand.*

(2) central processing electronics: the central processing electronics board contained the microprocessor and power supply, the RAM array with error-detection circuitry, the interrupt controller, the memory page decoder, the up clock and general timing functions, the memory-mapped I/O interface, and the central processing electronics extension. The main functions of the central processing electronics extension were to interface with the attitude control system bus, the Earth/Sun sensor, telemetry and telecommand, failure detection, timing and switching, and PROM supply;

(3) the PROM board: the configuration of the board was based on 8 k × 8 PROM chips providing a 16 k × 16 array for the central processing electronics. They were supplied through a switching system providing power only to the addressed chips;

(4) the sensor acquisition electronics: this module performed the analogue-to-digital conversion of the various analogue signals of the subsystem, by means of a front-end operational amplifier array, an analogue multiplexer and a 12-bit analogue-to-digital converter. The result of the conversion could be sent on the modular attitude control system bus, via a dedicated telecom controller and bus driver/receiver. Timing and switching functions, along with interface to internal buses, were also implemented;

(5) switching electronics: this board was the power interface to the relay coils. It was driven by the central processing electronics extension that sent the proper line and column addresses in compliance with the matrix organisation of this board. The relay status acquisition electronics was also implemented;

(6) DC/DC converter: the converter module provided the supply voltages required by the various control law electronics circuits, together with the relevant current limitation monitoring and power management capabilities. The circuit also supplied the Earth/Sun sensor. The electrical power was provided by the 50 V DC main and redundant buses, and primary and secondary power lines were isolated.

Control Actuation Electronics

The control and actuation electronics interfaced with the control law electronics, via the internal bus. Its functions were to condition the outputs of the sun acquisition sensors, the attitude anomaly detector, and the accelerometer package, to drive the reaction control subsystem latch valves, flow control valves, and catalyst bed heaters in response to commands from the control law electronics, to provide sensor power switching, to provide hardwired emergency attitude control modes during on-station operation, overriding the control law electronics, and to provide automatic fault detection and recovery during the spin-stabilised phase, initiating automatic reconfiguration of the control law electronics and reaction control assembly. Furthermore, it performed subsystem initialisation at separation.

The AC/DC converter module provided the proper power supply lines to the box, and it was connected to the data handling subsystem inverter as power source. The galvanic isolation requirement was met by means of shielded transformers connected to the two AC lines. The cross-strapping function was implemented at a secondary level, after the current limitation functions. A dedicated converter section, with serial regulators, was implemented to provide power to the accelerometer package.

The reaction control assembly was supplied directly from the 50 V DC lines through the high-power and pulse-capability current limit circuits, able to deliver to the valve coils the proper current pulse. The ‘failure detection electronics’ was the module in charge of failure detection and hardwired back-up mode management. Due to the failure recovery philosophy adopted, this module was not redundant. It implemented five failure criteria: active nutation damping failure detection, thruster impulse monitoring, and pressure anomaly detection in the spin-stabilised phase, and thruster impulse monitoring and attitude anomaly detection in the three-axis stabilised phase.

Any criterion, if verified, generated a reconfiguration signal that could be overridden by on-ground commands. Each failure detection electronics block was fully independent and was driven by proper enable/disable telecommands, in such a way that at any mission phase a dedicated failure detection strategy could be selected.

Accelerometer Package

The accelerometer package was used as nutation sensor during the spinning phase. It comprised three Sunstrand QA 2000-type accelerometers (A, B, and M) and the relevant conditioning circuitry. The A and B output signals were sent to the control law electronics through sensor acquisition electronics, in order to drive the software-based active nutation damping function. The M output signal was routed to the control and actuation electronics, to be used in the hardware-based active nutation damping failure detection.

Earth/Sun Sensor

The Earth/Sun sensor provided the attitude and spin-rate measurement during the first part of the mission, when the satellite was spin stabilised. It employed the Galileo sensor flown on many telecommunications satellites. The attitude determination was performed by correlating the cross times of the Sun into the two sun slits and measuring the length of the Earth chord, by means of the two infrared telescopes and a timing circuitry in the control law electronics.

Sun Acquisition Sensor

The sun acquisition sensors gave the attitude and orbit control system a rough estimation (1°.6 accuracy) of the sun aspect angle along two axes for sun acquisition purposes, both in the nominal case or for emergency sun reacquisition. Each sensor was made up of 8 photovoltaic cells (4 main, 4 redundant) delivering a current proportional to the cosine of the angle between the sun line and the normal to the cell surface. The actual sensor configuration gave a field of view of more than 2 steradians and the full set of three units gave a spherical coverage around the satellite. The load resistor and the conditioning electronics were in the control and actuation electronics.

Attitude Anomaly Detector

The attitude anomaly detector monitored the satellite attitude in order to avoid the possibility of the sun damaging the solar generator or the payload. The device was based on a solar cell inside a baffling system. In normal conditions (normal mode), the Sun should have stayed at about 43° sun aspect angle. If the sun aspect angle drifted from this value by more than 3°, the sensor would issue a current pulse that would trigger the attitude anomaly detector criterion in the control and actuation electronics failure detection circuitry, commanding a reconfiguration strategy.

13.3. Reaction Control Assembly

The reaction control assembly provided impulses for velocity corrections, for satellite positioning, spin-up and spin-down, and for attitude control. The assembly consisted of two separate, functionally independent sub-assemblies which were used sequentially: a hot-gas reaction control assembly, which used hydrazine (N_2H_4) propellant, and a cold-gas reaction control assembly, which used nitrogen propellant. Each sub-assembly incorporated two redundant and independent functional branches.

Hot-Gas Reaction Control Assembly

The hot-gas reaction control assembly was a conventional monopropellant hydrazine system. The propellant was stored in two identical tanks, which operated in a blow-down pressure mode over a range from 22 to 5.5 bar. The tanks did not contain any positive expulsion devices. The hydrazine was pressurised by gaseous helium. The propellant/pressurant interface required for positive propellant expulsion was maintained

by the centrifugal acceleration produced by the satellite spin. The tank shape was conospherical to maximise expulsion efficiency. Both tanks were fed and pressurised by a single fill and drain valve and a common feed line. The fill and drain valve incorporated a 25 μm filter. Another line linked the pressurant ports.

Four thrusters were required to meet the subsystem attitude control and velocity requirements. Hydrazine was fed through a flow control valve and was chemically decomposed through a catalyst-induced combustion process inside the thrust chamber. The hot gases expanded through a nozzle and produced thrust. Thrust chamber assemblies incorporated electrical heaters, which raised the catalyst temperature to approximately 190 °C, prior to hydrazine injection into the combustion chamber. The thruster branches could be isolated from either tank by latching-type isolation valves.

The thruster assemblies were protected from particulate contamination by one 10 μm filter, located between tanks and isolation valves. In addition, one 10 μm filter was installed in the inlet of each thruster propellant valve, in order to provide increased component protection. A pressure transducer was located immediately downstream of the propellant tanks. Its reading, combined with that of tank temperature sensors, provided information to establish the propellant mass inside the tanks, throughout the hot-gas reaction control assembly life. The propellant feed-lines consist of 6.4 mm outer diameter titanium tubing. Hydrazine tubing, tanks, latching, and flow control valves were insulated and thermally controlled in order to prevent the hydrazine temperature dropping below its freezing point, at approximately 2 °C.

Mechanical connections between feed-lines and thruster valves, latching valves, and pressure transducer, consisted of standard flare-type fittings; all other joints were TiG welded. Every item of equipment had been qualified for previous space programmes.

Cold-Gas Reaction Control Assembly

The cold-gas reaction control assembly was a pressure-regulated system, using gaseous nitrogen propellant. The nitrogen was stored at a maximum pressure of 285 bar in two equally sized tanks. The tanks were not interconnected, and separate fill and vent valves were used in order to pressurise the tanks. These valves incorporated a 5 μm filter. Each tank fed one pressure regulator, which reduced the gas pressure from tank level to an average of 1.5 bar.

Impulse for all manoeuvres was provided by one of two redundant branches of six thrusters each. Gas was fed from the pressure regulators to the two thruster branches through a system of four isolation valves. These latching type valves permitted the isolation of either thruster branch and its feeding by either regulator. During normal operation, only one regulator would be used to provide regulated pressure. A high pressure, 10 μm filter was installed upstream of each pressure regulator. In addition, integral filters were installed in the inlets of the regulators and the propellant valves to provide additional protection. The pressure regulator incorporated a relief valve which prevented over-pressurisation of the low pressure line. Over-pressurisation could occur in two instances: in the case of pressure regulator leakage and/or temperature effects during which the thrusters were not operated, or in the case of pressure regulator failure. In the worst case, the low pressure line could experience pressures similar to those in the high pressure lines.

To vent the resulting mass flow, a so-called 'zero thrust device' (a calibrated T-fitting) was installed near the pressure regulators, so as to minimise the impingement of gas on spacecraft units. In the case of pressure regulator failure, the gas that exited the spacecraft through its vents may have caused disturbance torques in the order of 10^{-3} to 10^{-4} Nm. The high-pressure transducers located in each branch of the sub-assembly and the tank temperature monitors provided the information needed to establish the propellant mass inside the tanks throughout mission life. Low-pressure transducers were included in each half of the sub-assembly, to measure the regulated pressure and monitor regulator operations.

The feed lines consisted of 6.4 mm outer diameter titanium tubing. Mechanical connections were made by TiG welding with the exception of the thruster assemblies, pressure regulators, pressure transducers, and latching valves, which were installed using standard flare-type fittings. Except for the 20 mN thruster, all equipment had been qualified for previous programmes. An extensive qualification programme was performed for the cold-gas thruster.

Operating Modes

The hot-gas reaction control assembly was to have been used at the start of the mission during the transfer orbit, near synchronous orbit, and the initial geostationary orbit operations. In practice the sequence of operations for the revised mission were quite different (see Chapter 4).

The hydrazine thrusters were used to spin up the satellite after separation from the launch vehicle from 7 rpm to 60 rpm in a series of manoeuvres. After this the satellite spin axis was oriented for the apogee boost motor firing. In the course of various attempts to ignite the apogee boost motor, the spacecraft was de-spun from 60 rpm to 30 rpm. During the de-spin manoeuvres, the hydrazine thruster also provided active nutation damping. After all further attempts to ignite the apogee boost motor had ceased, virtually all of the remaining hydrazine was used to increase the perigee height of the transfer orbit in a series of three manoeuvres. The spacecraft was then de-spun to 10 rpm and oriented with its spin-axis pointing at the Sun. A final orbit manoeuvre was performed to synchronise the orbital period with the satellite's rotation period. The residual liquid hydrazine was then expelled from the sub-assembly, in order to avoid mass shifts caused by hydrazine sloshing during nominal operating modes and, thus, to avoid unwanted attitude jitter.

The subsequent control forces were provided by the cold-gas reaction control assembly. The satellite was further despun, reoriented, and stabilised. Emergency manoeuvres during routine operations were also served by the cold-gas reaction control assembly.

A summary of the mission phases, the thrusters used, and the thruster operating modes is presented in Table 13.1.

Assembly Performance

The hot-gas reaction control assembly thrusters provided a nominal thrust of between 2–6 N, depending on the supply pressure. Nominal specific impulse during steady-state operations ranged between 215–225 s. During pulsed mode operation, the specific

Table 13.1. Reaction control assembly mission summary.

Mission Phase	Mode/Manoeuvre	Thruster(s)	Operating Mode	System
Pre ABM Firing	Spin up (to 60 rpm)	$+z$	continuous	hot gas
	Spin axis orientation	$\pm y$	pulsed	„
	Active nutation damping	$\pm y$	pulsed	„
Revised Mission	Spin axis orientation	$\pm y$	pulsed	hot gas
	Active nutation damping	$\pm y$	pulsed	„
	Perigee raising	$\pm x, \pm y$	continuous	„
	Spin adjustment	$\pm z$	pulsed	„
	Despin (60 to 10 rpm)	$-z$	continuous	„
	Orbit period adjustment	$\pm x, \pm y$	continuous	„
	Hydrazine expulsion	$\pm y, \pm z$	continuous, pulsed	„
	Final despin (10 to 0 rpm)	$-z$	continuous	cold gas
	Attitude acquisition	$\pm x, \pm y, \pm z$	continuous	„
	Nominal mode	$\pm x, \pm y, \pm z$	pulsed	„
	Attitude reacquisition	$\pm x, \pm y$	continuous	„

impulse dropped to ranges varying from 180–220 s to 85–110 s, depending on the duration of the pulse.

The cold-gas reaction control assembly thrusters provided a nominal steady-state thrust in the range 5–28 mN, depending on supply pressure and environmental conditions. Specific impulse during steady-state operations was 66 s or higher, and during pulse-mode between 60–70 s, depending on pulse duration.

Mass Budget

The reaction control assembly total dry mass, i.e. excluding propellant and pressurant, was about 29 kg. Usable hydrazine propellant mass was 32 kg. Residual, unusable hydrazine and pressurant mass amounted together to 0.65 kg. Usable nitrogen mass was 9.4 kg, the residual mass in tanks at the end of the operative mission being about 0.4 kg.

13.4. Inertial Reference Unit

Gyros provided continuous three-axis rate and incremental attitude data during final despin and the three-axis stabilised mission phases. The gyro package (see Figure 13.2) consisted of five inertial class rate-integrating gyros, gyros 1 and 3 aligned midway between the $\mp x$ and $+y$ axes respectively, gyro 2 along the $+x$ axis, and gyros 4 and 5 along the $\pm z$ axes respectively. The adopted configuration was optimised for adequate redundancy and to minimise disturbance torques. The rate and attitude information was provided by the gyro measurement electronics to the control law electronics, via the internal attitude and orbit control system bus.

The inertial reference unit was the satellite measurement device for attitude and angular rates during commissioning and normal mode phases. The output of this unit, together with star mapper data, were processed by the control law electronics software. In nominal operating mode the results influenced the output of the scientific mission; therefore, the inertial reference unit performances were of extreme importance for the satellite. The inertial reference unit of Hipparcos was a direct derivation from the one flying on the French Earth observation satellite SPOT. With the progressive failure of the gyroscopes, these functions were ultimately fully transferred to the spacecraft/payload, where the star mapper readings provided very high accuracy attitude sensing, albeit at a low frequency.

Based on a SAGEM GYPSE gyrometer, the inertial reference unit was split physically into two boxes, gyro package and gyro measurement electronics, and functionally into five measurement chains organised into three independent channels. The gyro package contained the gyrometers with their mechanical support, thermal insulation, and the thermal control electronics; the gyro measurement electronics contained the inertial reference unit power supply DC/DC converter (from 50V DC bus), the switching electronics, the telemetry and telecommand, and the modular attitude control system bus interface, the spin motor power supply, the pick-off supply, the rebalance loop, the clock and general timing function, and the so-called angular rate digital integrator that senses the current flowing in the rebalance loop and converts it into a pulse train at a frequency proportional to the angular rate seen on the input axis of the relevant gyrometer; with a proper accumulator register read at a fixed time, it was possible to obtain the required information on attitude and angular rate.

The main measurement characteristics of the inertial reference unit were: angular resolution 0.032 arcsec in fine mode, and 0.26 arcsec in coarse mode; a full scale of $0^{\circ}.125\ s^{-1}$ in fine mode and $0^{\circ}.83\ s^{-1}$ in coarse mode, and a constant drift of less than 2° per hour.

As a consequence of the revised mission orbit, the performance of the gyros in the high radiation environment to which the satellite was exposed started to degrade shortly after the launch.

13.5. Gyro Performances

The first gyro problems were traced back to November 1989 when increasing noise on gyro 4 (z axis) was observed. By mid 1990, the gyro deteriorated to the point where it had to be taken out of the control loop and replaced by the redundant one (gyro 5). Gyro 5 soon developed the same problems as gyro 4. In July 1992, it deteriorated to the point of affecting the spacecraft attitude and had to be taken out of the control loop. The new two-gyro software was then implemented (see Chapter 15). In September 1992 both gyro 2 and 5 showed anomalous behaviour. At the end of the month gyro 1 had several spin-downs and broke completely two weeks later, and was replaced by gyro 3. In December 1992 gyro 2 showed large spikes, breaking down in March 1993. An overview of the gyro performance during the mission is shown in Figure 13.3. A summary of the behaviour of the various gyros is given hereafter.

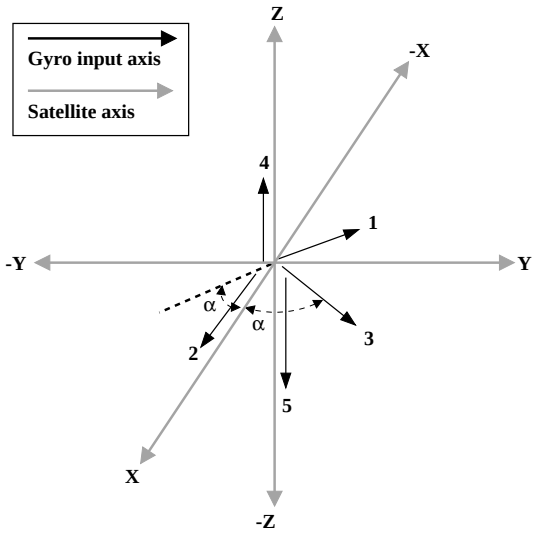

Figure 13.2. *The configuration of the five on-board gyros, illustrating the relationship between the gyro input axes and the satellite axes.*

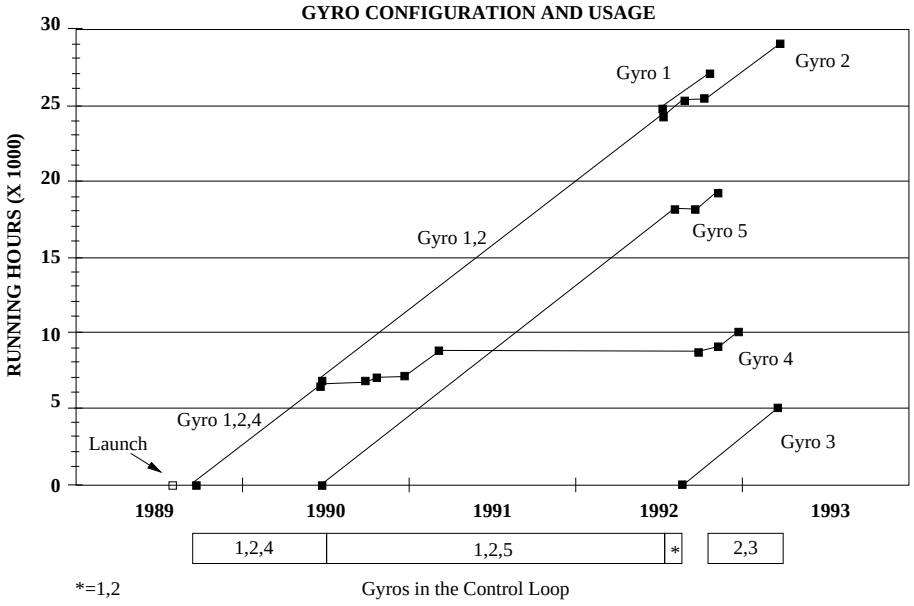

Figure 13.3. *The combination of gyros used at different stages of the mission. The bottom panel summarises which gyroscopes were operational during the mission. The upper panel indicates the cumulative running hours for each of the gyros. The two-gyro operations started towards the end of 1992.*

Gyro 1

July 92: Gyro 1 drift began to change erratically affecting real-time attitude determination performance.

92-09-25: The output of the gyro changed rapidly several times.

92-09-27: The output of the gyro again changed rapidly several times.

92-10-11: The gyro output went suddenly to zero. Several attempts were made to get the gyro working again, but with no success; finally the gyro was switched off. From that time, the gyro was used only for increasing the gyro measurement electronics box temperature as no real output could be obtained.

Gyro 2

92-08-11: The gyro was switched off by an automatic re-configuration order caused by an emergency sun reacquisition. The gyro was switched back on, but it developed the first spikes in the output and had to be switched off.

92-10-03: The gyro was switched off by an automatic re-configuration order caused by an emergency sun reacquisition. On the same day the gyro was switched on again, but there were several commanding problems due to the low gyro mechanical electronics box temperature; soon after the spikes in the output reappeared.

92-10-15: The gyro was switched off by an automatic re-configuration order caused by an emergency sun reacquisition. On the same day the gyro was switched on again, but soon after the spikes in the output reappeared. The same had to be repeated again later the same day due to a second emergency sun reacquisition.

92-10-27: The gyro output was tested via the gyro 2/5 de-multiplexing patch; this modification allowed the suppression of the output of gyro 2, gyro 5 or both.

92-10-13: The gyro output developed several spikes, but it recovered after the switch-off of gyro 5.

92-12-22: The spikes on the output of the gyro became severe enough to cause a loss of real-time attitude determination convergence outside perigee.

Gyro 3

91-07-28: During a regular gyro destorage, the gyro heater did not operate. The heater did not operate throughout the rest of the mission.

91-09-27: A test was conducted on the gyro to see if it would operate correctly at a lower temperature.

92-08-13: The gyro was switched on to replace gyro 2.

92-10-27: The gyro was switched off to allow the testing of gyros 2 and 5; it was turned back on at the end of the test.

Gyro 4

November 89: First noise on the gyro was observed.

90-06-26: The gyro output presented large variations for the first time.

90-06-29: The gyro was switched off and replaced by gyro 5.

90-10-18: A week long gyro destorage was started, where the gyro was left running outside the control loop.

90-11-15: During a normal gyro destorage, the output variations re-appeared several times.

90-12-20: During a normal destorage, the output did not change from zero and it took three attempts to finally get a correct spin rate. The gyro was then left on, but not in the control loop.

From 91-01-12 to 91-02-26: Occasional changes in the gyro spin rate caused the real-time attitude determination loop to diverge although it was not in the control loop.

91-03-01: The gyro was finally switched off.

92-10-04: Due to the problem with gyros 2 and 5, the gyro was switched on to get a correct spin-rate estimate. Then the gyro was switched off.

92-10-11: The gyro was again switched on.

92-10-27: The gyro was switched off.

92-11-13: The gyro was switched on to replace gyro 5 after an emergency sun reacquisition.

From 92-11-26 to 92-11-29: Gyro output variations were observed.

92-12-22: The gyro was finally switched off. On the same day, an emergency sun reacquisition occurred; the gyro was again switched on to increase the gyro mechanical electronics box temperature, but the output stayed at zero. After the temperature had stabilised, the gyro was switched off. From this day on, the gyro was used only for increasing the gyro mechanical electronics box temperature as no real output could be obtained.

Gyro 5

90-06-29: The gyro was switched on to replace gyro 4.

92-03: Deterioration on gyro 5 started to have a noticeable impact on overall real-time attitude determination performance.

92-07-03: The first large spikes occurred, causing the divergence of the on-board real-time attitude determination loop.

92-07-10: The gyro was taken out of the control loop but left on and was replaced by the two-gyro real-time attitude determination patch.

92-08-04: The gyro was switched off by an automatic reconfiguration order caused by an emergency sun reacquisition. The gyro was switched back on and large spikes were observed on its output.

92-08-08: Gyro 5 recovered sufficiently to return to three-gyro operations.

92-08-11: Scanning law acquisition manoeuvre return to 43° nominal scanning law. Glitches on gyro 5 output caused an emergency sun reacquisition. The spacecraft was then spun up and the gyro left off. From this day on, the gyro was not used again for the actual control of the satellite.

92-08-14: The gyro was switched on for a test and was then switched off again.

92-10-02: The gyro was switched on after an emergency sun reacquisition.

92-10-03: The gyro was switched off by an automatic reconfiguration order caused by an emergency sun reacquisition. On the same day, the gyro was switched on again but there were several commanding problems due to the low gyro mechanical electronics box temperature.

92-10-15: The gyro was switched off by an automatic reconfiguration order caused by an emergency sun reacquisition. On the same day, the gyro was switched on again with the same commanding problem experienced a few days earlier. It happened again later the same day due to a second emergency sun reacquisition.

92-10-27: The gyro output was tested via the gyro 2/5 de-multiplexing patch.

92-11-13: The gyro noise increased and the output indicated a spin-down to a level equal to 60 per cent of the nominal rate. After a check carried out with the star mapper output, the gyro was switched off.

92-12-22: After emergency sun reacquisition occurred the gyro was switched on to increase the gyro mechanical electronics box temperature, but the output stayed at zero. The gyro was left on, although the output had been disabled via the gyro 2/5 de-multiplexing patch and it was only being used to increase the gyro mechanical electronics box temperature.

Gyro Drift

Studies showed that on short timescales, gyro drifts were sensitive to long eclipses which gave rise to thermoelastic effects. During eclipses, the variation in drift for a thirty minute eclipse was approximately 10^{-7} arcsec s^{-1}. The estimated gyro drift over longer timescales (from the beginning of the mission) is illustrated in Figure 13.4. The larger discontinuities coincide with on-board gyro reconfigurations, since different operational gyros gave rise to different biases. The cause of the smaller variations was investigated. Thermal effects were believed to be the cause of this behaviour.

13.6. Gyro Related Ground Investigations

Ultimately the successive failures of the gyros was to lead to the complete redefinition of the on-board and on-ground real-time attitude determination systems using firstly two and then no gyros in the control loop (see Chapters 15 and 16 respectively). Before or in parallel with this development, a series of less drastic measures were taken to minimise the risk to the spacecraft of maintaining three-gyro operations.

Ground Procedures and Software Changes

In February 1991, while both gyro 4 and gyro 5 were switched on (with gyro 5 in the control loop), the specialised real-time attitude monitor software at ESOC was enhanced to perform limit checking on both gyros and to raise an alarm should the operational one go out of limits. The spacecraft controller would then have been able to swap the failing gyro out of the control loop before significant deviations from the nominal scanning law could accumulate, possibly leading to an autonomous triggering of the emergency sun reacquisition manoeuvre. This software was made largely redundant after gyro 4 was

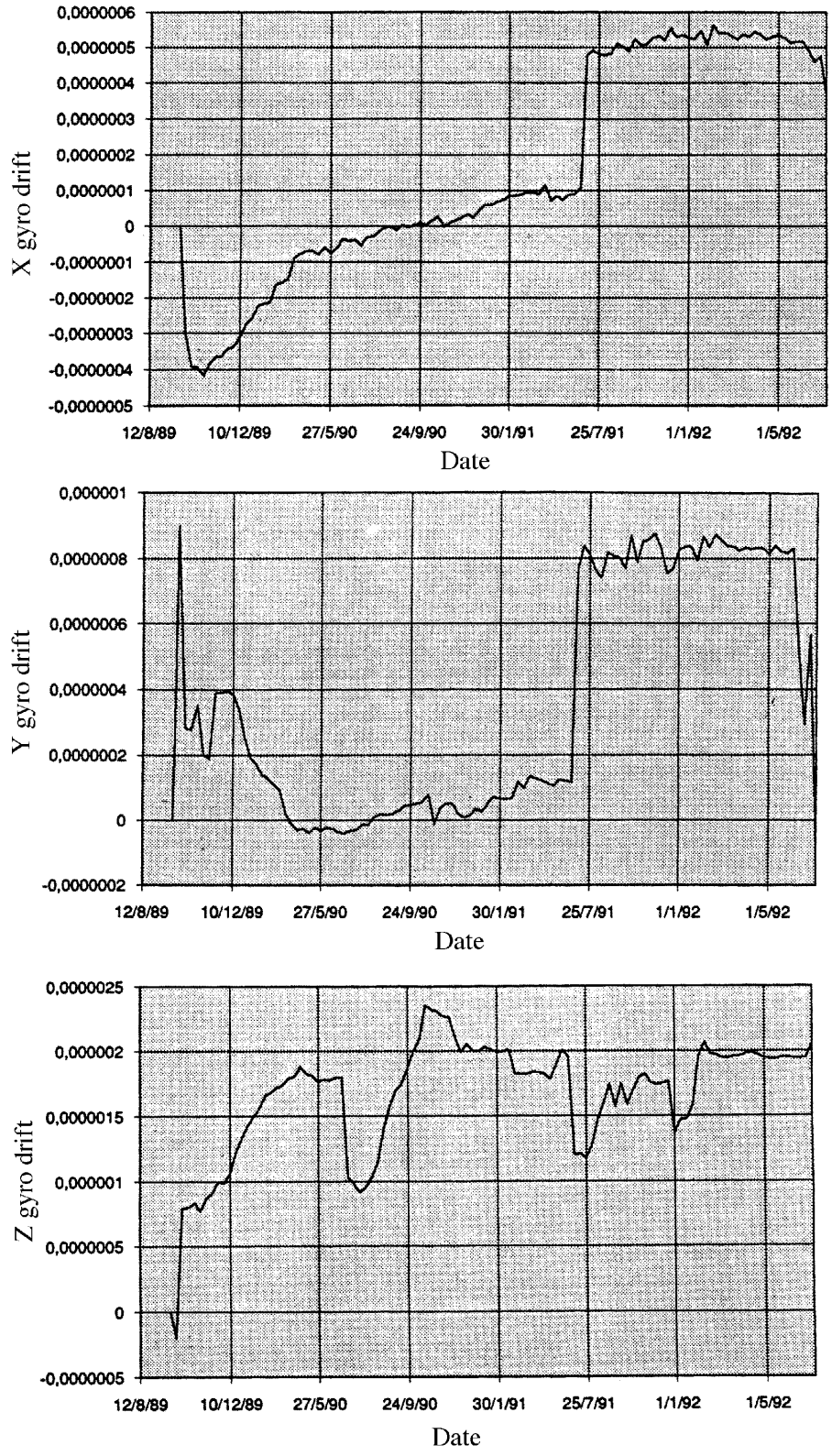

Figure 13.4. *Drifts for the x, y and z gyros (top to bottom), as estimated by the on-board real-time attitude determination system. The drifts are given in the on-board units of radians per AOCS cycle (16/15 s). The discontinuity in the drifts in July 1991 is associated with the upgrade of the orientation matrix for the gyros. The discontinuity in the z gyro drift in June 1990 is due to the change from gyro 4 to gyro 5.*

switched off and the monitoring of the gyro 5 output was achieved via the gyro 5 filter on-board software patch, described below.

In March 1992, in response to increased noise on gyro 5 having a detrimental effect on the real-time attitude determination performance, it was believed that any changes to the gyro drifts around perigee was most likely due to biased corrections by the real-time attitude determination (see Chapter 14). Therefore the ground procedures were changed to allow the resetting of the on-board drift estimates as soon as possible after perigee to the last values observed before perigee. Subsequent careful monitoring for drift evolution was then performed throughout the orbit to ensure that the best drift estimates were maintained.

Gyro 5 Filter On-Board Patch

Matra Marconi Space, as spacecraft prime contractor, were responsible for the development of a series of on-board software patches.

This patch was designed to reject all gyro 5 pre-processed outputs that were outside a given window (for example $168.^{\circ}75\ \mathrm{hr}^{-1} \pm 10^{\circ}$). In case a bad value was detected (outside the ground defined window) it was then replaced by the previous value. This patch became practically obsolete when the frequency of occurrence of bad values increased.

Gyro 2/5 De-Multiplexing On-Board Patch

Gyro 2 and 5 were part of the same inertial reference unit channel. It appeared that their output were at times swapped causing erroneous performance by the real-time attitude determination. A modification was then designed so that the software gave the option to read only one gyro output. This software became obsolete when the gyro electronic problem worsened and mechanical problems appeared.

Other Satellite Missions

In the case of Hipparcos the failures of the gyroscopes were characterised by high output noise, high amplitude output spikes, repeated spin-rate anomalies, followed (except for one out of five gyroscope systems) by a final spin-down. The thermal control of the remaining gyroscope system failed and its output was severely degraded.

Hipparcos was not the only mission to be affected in an adverse manner by failure of the gyroscope systems. Three of the four gyroscope systems on board the German satellite ROSAT showed output transients whose polarity was correlated with the immediately preceding angular manoeuvre. Two gyroscope systems exhibited apparent spin-rate anomalies, leading to final spin-down for one of them. However, similar gyroscope systems flying on other European satellites showed very few in-orbit anomalies.

An inter-agency ‘gyroscope systems working group’, maintained by ESA, CNES (F), DARA (D), and DRA (UK) from 1992 until mid-1993, conducted systematic investigations of Hipparcos and ROSAT flight data through contracts placed with gyroscope manufacturers. These investigations were later supported by the Laboratoire de Recherches Balistiques et Aérodynamiques (F). A general conclusion reached by all parties to the

investigation was that the primary source of all the failures lay in the electronics of the gyroscope system and not in its electro-mechanical gyroscope unit.

The in-orbit failures of the Hipparcos satellite were investigated by Matra Marconi Space, who integrated the inertial reference unit and supplied most of the gyroscope electronics, and SAGEM (F), the gyroscope manufacturer. All anomalous behaviour and failures of the gyroscope systems could be explained in terms of radiation-induced degradation of electronic components. This was deduced from the abnormal orbit flown and the time which elapsed before the most serious failures were observed, about three years after launch, after the nominal lifetime had expired.

Causes of failure were traced to the spin motor supply circuitry, while other failures were thought to have most probably originated in sensitive electronic interfaces. Anomalies occurring in the ROSAT satellite were investigated by GEC-Ferrari (UK). These concluded that the most probable cause of failure was the electronic circuitry supplying the spin motor, although other electronic failures were also noted. The recommendations for improving gyroscope systems, resulting from this inquiry, were passed to ESA projects and industry.

13.7. Gas Consumption

The cold-gas mass (M_{cg}) in the tanks was calculated as follows:

$$M_{cg} = \frac{PV}{zrT} \qquad [13.1]$$

where P is the tank pressure (Pa), V is the tank volume (m^3), z is the compressibility factor for nitrogen, T the temperature (K) and r a constant. The evolution of the cold gas, since October 1989, is shown in Figure 13.5. By May 1992 tank 1 was almost empty, with only 0.6 kg remaining. Tank 2 still had 4 kg out of the original 5.07 kg.

The average consumption was 0.15 kg per month. The consumption followed a linear law. Extrapolating that law predicted an attitude and control ability until after 1994, well beyond the final termination of satellite operations in August 1993.

13.8. Normal Mode Controller

The primary output from the on-board real-time attitude determination system (see Chapter 14) were the estimated angular deviations from the nominal scanning law (error angles) and their rates of change (error rates). These error angles and error rates were combined within the 'normal mode' control software to produce error signals. When an error signal exceeded the preset threshold level, thruster firings were commanded on all three axes. The lengths of the pulses were determined as a function of the angles, rates and a preset estimate of the disturbance torque.

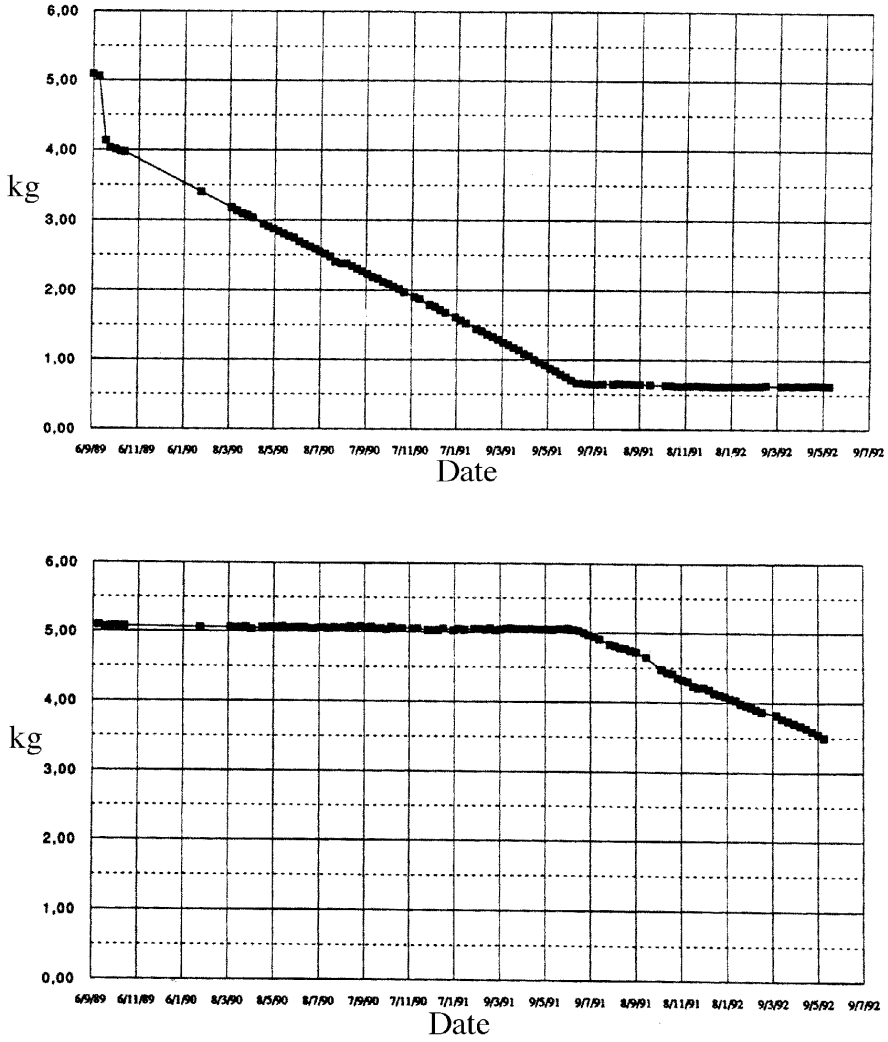

Figure 13.5. *Hipparcos cold gas consumption: (a) tank 1 and (b) tank 2.*

On-board Disturbance Torque Modelling

The disturbance torque estimates were based on the assumption that the satellite would operate from a geostationary orbit. Therefore the on-board disturbance torque model was designed to give a first-order estimate only, based on the expected predominant torques, i.e. a constant torque arising from the moments of the spinning gyros, and a periodic torque arising from radiation pressure. In practice, other torques such as gravity gradient, magnetic torques, and atmospheric drag (near to perigee) played a very significant role at lower altitudes resulting in modifications to the normal mode control around perigee.

The radiation pressure torque varied according to the geometric surfaces of the spacecraft which were exposed to sun-light. Consequently, the torques around the spacecraft x and y axes had a periodicity equal to that of the spacecraft rotation rate (2 hours 8 min). Due to the approximate 120° rotational symmetry of the spacecraft about the z axis, the radiation pressure torque around the z axis had a periodicity of 1/3 of the spacecraft rotation period. It was sufficient for the normal mode control to assume a sinusoidal model for the radiation pressure torque.

The orbital oscillator parameters, $S_v(k)$, $C_v(k)$, described in Chapter 8, were used to model the phase angle of the periodic torques around the x and y axes. For the z axis, a further two phase angle parameters were required. Recalling that $S_v(k)$ and $C_v(k)$ are the sine and cosine of phase angle $\Omega_d t_k$ respectively, it was possible to model the disturbance torques around the z axis using a phase angle of $3\Omega_d t_k$. Therefore the on-board computer was capable of evaluating:

$$\begin{aligned} S_{v3}(k) &= \sin(3\Omega_d t_k) \\ C_{v3}(k) &= \cos(3\Omega_d t_k) \end{aligned} \qquad [13.2]$$

by addition and multiplication only, using the standard trigonometrical expansions of $\sin(3\theta) = \sin((\theta + \theta) + \theta)$ (similarly for cosine).

On-board Algorithm

The following variables (updated every $\frac{16}{15}$ s) were input from other areas of the control software:

$\phi(k)$, $\theta(k)$, $\psi(k)$: x, y and z error angles from real-time attitude determination (see Chapter 14).

$\dot{\phi}(k)$, $\dot{\theta}(k)$, $\dot{\psi}(k)$: x, y and z error rates from real-time attitude determination.

$S_v(k)$, $C_v(k)$, $S_{v3}(k)$, $C_{v3}(k)$: Orbital oscillator outputs (see Chapter 8 and above).

The following on-board constants were used:

K_x, K_y, K_z: X, Y and Z rate gains

μ_x, μ_y, μ_z: X, Y and Z thresholds

A_x, A_y, A_z: coefficients of ϕ_k, θ_k, ψ_k

B_x, B_y, B_z: coefficients of T_x, T_y, T_z

C_x, C_y, C_z: coefficients of $\dot{\phi}_k$, $\dot{\theta}_k$, $\dot{\psi}_k$

T_{xc}, T_{yc}, T_{zc}: constant disturbance torque estimates

T_{xss}, T_{yss}, T_{zss}: disturbance torque sine coefficients

T_{xsc}, T_{ysc}, T_{zsc}: disturbance torque cosine coefficients

Defining additionally:

ϵ_x, ϵ_y, ϵ_z: error signals

T_x, T_y, T_z: external disturbance torque estimates

$t_{\mathrm{on},x}$, $t_{\mathrm{on},y}$, $t_{\mathrm{on},z}$: calculated on-times

the error signals were given by:

$$\begin{aligned} \epsilon_x &= \phi_k + K_x \dot{\phi}_k \\ \epsilon_y &= \theta_k + K_y \dot{\theta}_k \\ \epsilon_z &= \psi_k + K_z \dot{\psi}_k \end{aligned} \qquad [13.3]$$

The thruster on-time calculation was only performed if an error ϵ exceeded in magnitude its corresponding threshold μ.

(i) Disturbance torque estimates:

$$\begin{aligned} T_x &= 2\ T_{xc} + T_{xss}\ S_v(k)\ T_{xsc}\ C_v(k) \\ T_y &= 2\ T_{yc} + T_{yss}\ S_v(k)\ T_{ysc}\ C_v(k) \\ T_z &= 2\ T_{zc} + T_{zss}\ S_{v3}(k)\ T_{zsc}\ C_{v3}(k) \end{aligned} \qquad [13.4]$$

(ii) On-time calculation:

$$\begin{aligned} t_{\mathrm{on},x} &= A_x\ \phi_k + B_x\ T_x + C_x\ \dot{\phi}_k \\ t_{\mathrm{on},y} &= A_y\ \theta_k + B_y\ T_y + C_y\ \dot{\theta}_k \\ t_{\mathrm{on},z} &= A_z\ \psi_k + B_z\ T_z + C_z\ \dot{\psi}_k \end{aligned} \qquad [13.5]$$

At the start of the mission, an upper limit of 500 ms and a lower limit of 50 ms was imposed on any calculated on-time.

Ground Disturbance Torque Calibration

The disturbance torque coefficients T_{xc}, T_{yc}, T_{zc}, T_{xss}, T_{yss}, T_{zss}, T_{xsc}, T_{ysc} and T_{zsc} were regularly calibrated on ground and uplinked at the same time as the orbital oscillator coefficients. The torque estimation was performed by fitting sine curves to the measured angular accelerations derived from gyro data. In the course of the mission, this ground based calibration was enhanced to include gravity gradient torques, thereby allowing accurate calibrations to be performed over more of the orbit. Ultimately, this disturbance torque estimation procedure underwent significant modification for the two-gyro operations (Chapter 15).

Perigee Control

As mentioned above, the disturbance torques around perigee were arising from other effects such as gravity gradient and atmospheric drag. Consequently, the disturbance torque model was redundant in this region and the on-times had to be much greater to combat the torques encountered. A different set of on-time coefficients were set on-board before each perigee passage. In particular, the coefficients B_x, B_y, B_z were set to zero and the values of C_x, C_y, C_z were increased.

13.9. Thruster Monitoring and Normal Mode Software Patch

At the start of the mission, particular attention was paid to fuel consumption around perigee, since the mission lifetime could have been decided on cold-gas consumption. Early in 1990, the on-ground real-time attitude monitoring software was modified to give extra thruster performance monitoring. As a result of this and other studies, the altitude at which the switch from normal mode to perigee mode control occurred was optimised to minimise ‘double-sided’ firings. Such double-sided firing occurred when the perigee control software commanded too large an actuation causing a rapid change in error signal from one error threshold to the other. This was indicative of inefficient control. However, the perigee control parameters could not readily be made weaker since they would have to command long enough actuations to avoid continuous and

inaccurate control at closest perigee approach. Another aspect of both the normal and perigee control software was the coupling of actuations around all three axes. Although less efficient in fuel consumption, this coupling was effected to allow longer periods of science observations without the jitter caused by an actuation.

However, as the data reduction consortia began to process the science data it was noticed within their own on-ground attitude reconstitution, that the small actuations around the z axis which were being commanded because the x and y error signals were hitting the threshold were very often entirely superfluous, wasting fuel and hindering the derivation of accurate scan-rate measurements.

Subsequently, Matra Marconi Space were commissioned to produce an on-board attitude and control software patch called the 'z thrusters de-coupling and accumulator patch', consisting of two different modifications to the normal mode controller. The first change compared the computed z thruster on-times with a given threshold, and if this was not exceeded, no firing was actually performed. The second modification accumulated all z thruster on-times and compared them with another threshold; when the given value was exceeded, the software inhibited the z normal mode control (no further firings allowed). This was to avoid excessive z-thrust (spin-up/spin-down of the spacecraft) in case of a z-gyro failure. As this could possibly have occurred outside ground station contact, it avoided the possibility of a significant loss of propellant as a result of a single failure. Both thresholds could be modified and reset via ground commands. The hardwired on-board safety protection had been disabled because of the nature of the orbit.

13.10. Disturbance Torques

The third attitude and control software modification developed by Matra Marconi Space, the 'spy' patch, allowed the storage of N words (16 bits) each cycle of the attitude and control software memory. These data were stored in a random access memory (RAM) area specified by a low and a high limit. This could be dumped using the normal attitude and control software dump routine. The patch had been primarily developed to gather data around the non-visibility periods (perigee) in order to obtain more information about the torques acting on the spacecraft causing attitude divergences almost every perigee. The nature of the disturbance torques is discussed fully in Volume 3, Chapter 8.

13.11. Real-Time Attitude Determination

The definition of the revised mission and the subsequent performance of the attitude and orbit control system hardware had a profound effect on the performance of the on-board real-time attitude determination system as well as the ground real-time attitude determination system used for initialisation of the on-board system. In particular, the failures of the gyros led to major re-design work being required on both systems. The three gyro systems, upgrades and re-design for two- and zero-gyro operations are described fully in Chapter 14 (three gyros), Chapter 15 (two gyros) and Chapter 16 (no gyros).